1   ANATOMICAL STRUCTURE OVERRIDE**S** TEMPERATURE CONTROLS ON

2   MAGNESIUM UPTAKE - CALCIFICATION IN THE ARCTIC/SUBARCTIC

3   CORALLINE ALGAE *LEPTOPHYTUM LAEVE* AND *KVALEYA EPILAEVE*

4   (RHODOPHYTA; CORALLINALES)

5

6   Merinda C. Nash

7   Walter Adey

8   Department of Botany, National Museum of Natural History, Smithsonian Institution,

9   Washington, DC, USA, 20560

10

11   Author for correspondence: nashm@si.edu

12   Running title: Magnesium and anatomy in coralline algae

13   Key words: Coralline algae, calcification, biomineralization, magnesium, temperature,

14   proxy

15

16

17   Abstract

18

19   Calcified coralline red algae are ecologically key organisms in photic benthic

20   environments. In recent decades they have become important climate proxies, especially

21   in the Arctic and Subarctic. It has been widely accepted that Magnesium content in

22   coralline tissues is directly a function of ambient temperature, and this is a primary basis

23   for their value as a climate archive. In this paper we show for two genera of

24   Arctic/Subarctic corallines, *Leptophytum laeve* and *Kvaleya epilaeve,* that previously

25   unrecognized complex tissue and cell wall anatomy bears a variety of basal signatures for

26   Mg content, with the accepted temperature relationship being secondary. The

27   interfilament carbonate has lower Mg than adjacent cell walls and the hypothallial cell

28   walls have the highest Mg content. The internal structure of the hypothallial cell walls

29   can differ substantially from the perithallial radial cell wall structure. Using high-

30   magnification Scanning Electron Microscopy and etching we expose the nm-scale

31   structures within the cell walls and interfilament. Fibrils concentrate at the internal and

32   external edges of the cell walls. Fibrils ~10 nm thick appear to thread through the radial

33   Mg-calcite grains and form concentric bands within the cell wall. This banding may

34   control Mg distribution within the cell. Similar fibril banding is present in the

35   hypothallial cell walls but not the interfilament. Climate archiving with corallines can

36   achieve greater precision with recognition of these parameters. This paper is part of a

37   series of investigations on controls on Mg uptake and distribution within the crusts of a

38   range of coralline genera.

Introduction

40   Understanding tissue complexity and the structural organization of cell wall calcification

41   in coralline algae is important for many reasons, including the growing use of these

42   organisms as climate proxies and concern for the ecological effects of ocean acidification.

43   There is a burgeoning interest in using coralline crusts as environmental proxies for late

44   Holocene temperature (Hetzinger et al. 2009, Gamboa et al. 2010, Halfar et al. 2010),

45   arctic ice sheet coverage (Halfer et al. 2013) and pH changes with time (Krayesky-Self et

46   al. 2016). Typically magnesium content is used as a key indicator of late Holocene

47   temperature fluctuations (Adey et al. 2013). Yet despite this utilization of coralline

48   carbonate crusts for proxy climate research, there has been little study of tissue and

49   cellular-scale physiology as it relates to the distribution of magnesium within the crust.

50   Nor are the basic mechanisms of calcification fully understood (Adey 1998). This is in

51   stark contrast to the status of other calcifiers used for proxy work, e.g. corals (Barnes and

52   Lough 1993), foraminifera (Bentov and Erez 2005) and bivalves (Wanamaker et al. 2008).

53   However, these well-known climate proxies have little application in the Arctic Region

54   of greatest climate change affects (Adey et al. 2013), and without a greater understanding

55   of coralline calcification physiology, precision proxy analysis of temperature and other

56   environmental conditions, using coralline algae, is limited.

57

58   One of the key roles of corallines is the building of carbonate substrate that underpins

59   many ecosystems globally. For example, the thick bioherms found in coral reef

60   structures (Adey 1978a, b, 1998), the extensive rhodolith beds off South American

61   (Amado-Filho et al. 2012, Bahia et al. 2010) and Australian (Harvey et al. 2016) shores,

3

62   maerl substrate in the Mediterranean (Martin et al. 2014) and the dominant rocky benthos

63   biostromes and rhodoliths in many Arctic and Subarctic environments (Adey et al. 2013).

64   There are concerns that as atmospheric $p\mathrm{CO_2}$ increases and consequent ocean

65   acidification increases, there will be negative impacts on the capacity of corallines to

66   continue building these important substrates (e.g. McCoy and Kamenos 2014). The pace

67   of research on the effects of temperature and climate change on coralline algae has

68   outpaced both the published data on anatomy and our understanding of the biochemical

69   processes controlling their carbonate skeletal building. For developing reliable past

70   climate proxy information using corallines and anticipating future climate change impacts

71   on these keystone calcifiers, as with any other organism, it is first necessary to understand

72   how these algae organize their tissues, build their skeleton and control cellular-scale

73   magnesium content.

74

75   While numerous studies of coralline growth rates under a wide range of temperature and

76   light conditions have been published (Adey and McKibben 1970, Adey 1970, 1973, Adey

77   and Vassar 1975), little attempt has been made to relate this information to calcification

78   processes. Also, it is only recently, with the use of higher magnification scanning electron

79   microscopy (SEM) (Adey et al. 2005, 2015) that the earlier implications of anatomical

80   complexity (Adey 1964, 1965,1966a) have been fully appreciated. It has been proposed

81   that calcification is a result of locally elevated pH during photosynthesis leading to super-

82   saturation and associated mineral precipitation (Ries 2010). However, some parasitic

83   corallines lack photosynthetic pigments, and have haustoria to derive nutrition from their

84   hosts, yet present typical tissue and calcified wall structures (Adey and Sperapani 1971,

85   Adey et al.1974). Also, anatomical and magnesium content studies of Arctic corallines

86   demonstrate that growth continues in Arctic winter darkness (Halfar et al. 2011, Adey et

87   al. 2013). There has been an experiment recording continued calcification at night and in

88   the dark (experiment in progress) indicating that calcification is not likely a straight

89   forward association with micro-saturation state, as seen in some algae (e.g., *Halimeda*,

90   Adey 1998, Sinutok et al. 2012).

91

92   Following on from the classical coralline studies, maturing around the turn of the 19th

93   century, Adey (1964, 1965,1966a,b) laid out the basic tissue-structured anatomy of

94   crustose corallines, adding the epithallium, intercalary meristem and cellular elongation

95   (while calcified) to the classical model of perithallium and hypothallium. Later, SEM

96   (Adey et al. 2005, Adey et al.2012) demonstrated greater sub-tissue complexity and

97   added the calcified cell wall components inner wall (IW) and interfilament (IF). In this

98   paper, we rename the inner wall the cell wall and retain the terminology interfilament,

99   noting this is equivalent to the middle lamella in higher plants (Esau 1953); interfilament

100   has also been referred to as interstitial (Ragazzola et al. 2016). We use the abbreviations

101   PCW and PIF (perithallial cell wall and perithallial interfilament) and HCW and HIF

102   (hypothallial cell wall and interfilament) to designate the carbonate wall components. It

103   should be noted that while the interfilament is a minor component of total calcification in

104   the species of this paper, it can be a major component in some genera (Adey et al. 2013,

105   2015a).

106

107   In this paper, we show for the first time the cellular-scale and anatomical controls on

108   magnesium distribution within the carbonate skeletons of two Arctic/Subarctic coralline

109   species. These are *Leptophytum leave* (Stromfelt) Adey, and the epiphytic (and non-

110   photosynthetic parasitic) *Kvaleya epilaeve* Adey and Sperapani, from the northern

111   Labrador Coast. *L. leave* is photosynthetic and forms expansive, but thin crusts (to one

112   mm in thickness) generally on shell fragments and pebbles in deeper water (Adey 1966a,

113   1970). *K. epilaeve* is an epiphytic parasite, lacking in photosynthetic pigment, and

114   producing hypothallial haustoria that penetrate upper perithallial cells of *L. leave* (Adey

115   and Sperapani 1971). It is similar in physiology to the North Pacific Subarctic parasite

116   *Ezo epiyessoense* (Adey et al.1974), which, along with its host *Lithophyllum yessoense*,

117   lies in a distantly related coralline group. *K. epilaeve* is the only known Arctic genus of

118   algae (Adey et al. 2008) and is absent or of very limited occurrence in Subarctic waters,

119   where the host continues to be abundant (Adey and Sperapani 1971). Understanding and

120   contrasting calcification within these two species, both growing in the same temperature,

121   light and pH conditions, offers an opportunity to examine the wide variance of Mg

122   content as a function of skeletal anatomy and metabolic processes.

123

124   **Methods**

125   *Sample collection and site information*

126   The sample was collected on 22nd July 2013, at the commencement of Arctic summer,

127   from 16-18 m depth at inner Port Manvers Bay, Labrador. The collection site lies at 56º

128   57.1' N; 61º 32.8' W., near the northern end of the 50 km long Port Manvers Run, a

129   north/south passageway inside of S. Aulatsivik Island (Fig. 1A). Sea ice is extensive from

130   November through early July, and the inter-island passages and bays are covered with

131   snow-covered land fast sea ice through much of that period. At the collection site, the

132   bottom was a shell/pebble gravel bed primarily of shell fragments and pebbles encrusted

133   with *L. leave*, *L. foecundum* and *Clathromorphum compactum*; scattered coarse rhodolith

134   *Lithothamnion glaciale* and *Lithothamnion tophiforme* were also present (Fig. 1B). *K.*

135   *epilaeve* occurred on *L. leave* and *L. leave* grew on both sides of the shell fragments.

136   Salinity was measured using electronic induction instrumentation and was 30 ppt.

137   November to July near surface water temperatures, below the sea ice, are within the -1.5

138   to -1.8º C range. Bottom summer temperature measured at the site on 22nd July 2013 was

139   0.5ºC. Since this is relatively early in the summer season, peak temperatures are likely to

140   be between 3-5ºC (Adey et al. 2015) with a mean growing season temperature of ~ 2 º C.

141   This mean estimate is based on measurements from eight sites in the region (182 km S to

142   35 km N) with surface to bottom temperature records for 1964 (Adey 1966c) and 2013

143   (Adey et al. 2015). These ranged from 1.9 to 5.6º C during summer at 15-20 m. The

144   snow-covered land fast sea ice overlying the gravel rhodolith bed from which the samples

145   were taken likely precludes significant solar energy from reaching the bottom for eight

146   months of each year.

147

148   Species identification was made by WHA.   The original sample is 2013-11(1) at the

149   National Museum of Natural History.

150

151   **Analytical methods**

152   *Scanning electron microscopy- energy dispersive spectroscopy (SEM-EDS)*

153   The CCA sample was fractured, mounted using carbon tape and platinum coated prior to

154   scanning electron microscopy energy dispersive spectroscopy (SEM-EDS). For these

155   analyses, we used a Zeiss UltraPlus field emission scanning electron microscope

156   (FESEM) equipped with an HKL electron backscatter diffraction (EBSD) operated at 15

157   kV, 11 mm working distance. SEM was carried out at the Australian National University

158   Centre for Advanced Microscopy. SEM-EDS was used for spot analyses to quantify the

159   elemental composition of representative parts of the CCA crust. A range of SEM settings

160   were used for imaging. The more common secondary (SE) electron showing topography,

161   backscatter electron imaging (BSE) which shows higher magnesium areas as darker

162   carbonate and is useful for rapid visual identification of mineral distribution.

163

164   A second round of EDS was undertaken using a NOVA NanoSEM FEI at the National

165   Museum of Natural History's Department of Mineralogy. Typically EDS measurements

166   are made using 15 kV (Nash et al. 2011) so that there is enough energy to dislodge

167   electrons from a range of elements, e.g. from lighter magnesium up to heavier strontium.

168   The EDS beam interacts with a roughly spherical-shaped region of carbonate beneath the

169   surface. This region is referred to as the interaction volume. At 15 kV the interaction

170   volume is ~ 3 μm in diameter whereas the average cell wall thickness ranges from only

171   500 nm up to ~2 μm (occasionally thicker, up to 3 μm). Interfilament in these species

172   may be only a few grains wide, 200-500 nm up to 2 μm. These narrow areas of interest

173   in contrast to the larger beam interaction volume, pose a problem for obtaining accurate

174   Mg measurements for only cell wall or interfilament. For example, a measurement of the

175   cell wall may include minor amounts of carbonate from the adjacent interfilament and

176   vice versa. Generally even with this beam crossover, in our experience 15 kV is sufficient

177   to identify a significant offset in magnesium while still collecting information that may

178   be of interest such as strontium levels. However, where there are only a few grains of

179   interfilament, as in the *L. leave,* the 3 μm interaction volume is problematic. A range of

180   EDS settings were tested aiming to reduce the beam interaction volume so that Mg

181   content for each the cell wall and the interfilament could be individually measured

182   without the beam crossing into the adjacent substrate. A setting of 7 kV, working distance

183   6.4 mm and 1 nA current was used to measure the interfilament grains in the *l. leave* with

184   a count time of 20 seconds. The sample was carbon coated. This was calculated to have

185   an interaction volume of <1 μm. These results are reported separately to the main data

186   set.

187

188   *Sample preparation*

189   Initially the crust was fractured using shears and mounted in superglue. After first

190   imaging of the fractured crust, the sample was polished using 2000 gsm wet and dry

191   sandpaper then sonic cleaned in unbuffered deionized water for 2 minutes. This

192   preparation was used for SEM EDS measurements; 8-9 measurements were made for

193   each carbonate type of interest. Subsequently the sample was sonic cleaned in unbuffered

194   deionized water for 20 minutes. The deionized water has a pH of ~6.5. When cleaned

195   for 2 minutes the surface is very lightly etched allowing differentiation between different

196   Mg-calcite morphologies without altering the measured Mg content. After cleaning for

197   20 minutes there is a visible difference in the surface with much of the interfilament Mg-

198   calcite and smaller grains removed allowing imaging of nm scale cellular structures.

199

200   X-ray diffraction methods

201   Powder XRD was carried out using a SIEMENS D501 Bragg-Brentano diffractometer

202   equipped with a graphite monochromator and scintillation detector, using CuKα radiation.

203   A subsample was broken off the edge of the crust. This piece included *L. leave* with

204   surficial *K. epilaeve*. The sample was ground using a mortar and pestle. Fluorite was

205   added as an internal standard. The sample was not bleached and acetone was not added

206   during the grinding as this has been found to occasionally induce alteration and

207   precipitation of other minerals in other coralline samples we have worked with. Scan

208   interpretation for mol% $MgCO_3$ followed the methods described by Nash et al. (2013).

209

210   *Temperature calibration*

211   Data for the graph in figure 5 taken from Halfar et al. (2010, 2013).

212

213   **Results**

214   *SEM imaging overview*

215   The specimen of *L. laeve* encased an aragonite carbonate shell. (Fig. 2A). The crust is

216   approximately 500 microns thick (Fig. 2B) with a basal hypothallus ~80 microns thick. *K.*

217   *epilaeve* has been considered to be an adelphoparasite, a species very closely related to its

218   host. Although diminutive, and superficially appearing as scattered white sand grains, *K.*

219   *epilaeve* can densely coat *L. leave*. Although often appearing as densely crowded

220   conceptacles, it can possess the full basic array of anatomical features: hypothallium,

221   perithallium and epithallium (the latter mostly absent, Adey and Sperapani 1971) (Fig.

222   2B). *L. laeve* typically has an epithallium that is one cell layer of rounded ovoid, thin

223   walled cells that are often absent in SEM sections. The *K. epilaeve* grows directly on the

224   *L. laeve* meristem (Fig. 2C, D) and there was no evidence of excavation required (by

225   borers or grazers), prior to settlement. This suggests that unlike the typical sloughing

226   relationship with epiphytes wherein epithallium builds up under the epiphyte until it

227   sloughs off, the *L. leave* does not recognize *K. epilaeve* as foreign. The perithallial cell

228   walls of *L. laeve* contain radially-oriented grains of Mg-calcite; the interfilament is thin

229   and has carbonate grains randomly orientated in a plane parallel to the filament axis or

230   cell top/ bottom. The interfilament shows up strongly as stripes on vertical fracture

231   sections (Figs. 2B, C). Note for easiest viewing of the fine structures, the figure images

232   are best viewed on screen rather than in print.

233

234   The first layer formed by the *K. epilaeve* has angular grains parallel to the *L. laeve*

235   surface (Fig. 2E). The bottom part of the cell wall is without radial structure and has

236   submicron beads appearing to calcify along and within organic fibrils (Fig. 2E). Organic

237   fibrils are visible between the basal layer of *K. epilaeve* carbonate grains and the

238   meristem of the *L. leave* (Fig. 2F) suggesting a method of attachment in addition to the

239   haustoria developed by some hypothallial cells (Adey and Sperapani 1971). There were

240   no haustoria visible in our SEM sample. Fine radial grains typically observed in cells of *L.*

241   *leave* beneath the meristem were not apparent in the cell walls of the *L. laeve* meristem

242   (Fig. 2E,F) suggesting this surficial carbonate may have been altered or remineralised

243   during the attachment process.

244

245   *SEM-EDS*

Biogeosciences
Discussions

Open Access

246   Measurements for magnesium content in *Leptophytum leave* were undertaken on both the

247   upper (side with conceptacles) and under (without conceptacles) crusts (Fig. 2A, D). The

248   parasite, *Kvaleya epilaeve* was present on both surfaces (Fig. 2A, Fig. 3A, B).

249   Measurements of *K. epilaeve* were made on the underside.

250

251   The Mg content of the perithallial and hypothallial cell walls of *L. leave* was measured

252   (Fig. 2 A-D) as well as what appeared to be a transitional cell type between the basal

253   hypothallus and the typical perithallial cells (Fig. 2 D-F). These transitional cells are

254   within the perithallus but have thin cell walls similar to the hypothallial cells. There are

255   clear visual differences between the cell walls of the three cell types. The perithallial cell

256   walls are 1-2 microns wide with clearly radial Mg-calcite (Fig. 2B, F). The basal

257   hypothallial cells are elongated relative to the perithallial cells and their cell walls are

258   narrower and do not always show radial cell wall structure (Fig. 2C). The transitional

259   cells have elongate cells relative to the perithallus but less so than the hypothallus, and

260   their cell walls are thinner, $\sim 0.5 - 1$ micron and do not show radial structures. The

261   interfilament of *L. laeve* has only a single layer of Mg-calcite grains (Fig. 2B, F), as noted

262   above showing as a thin line on longitudinal axial fractures; fractures along the

263   interfilament appear as conspicuous vertical stripes (Figs. 2C).

264

265   The *K. epilaeve* in the portion of the sample mounted for SEM did not present the typical

266   elongated hypothallial cells as shown by Adey and Sperapani (1971), as this cut is not

267   longitudinally placed on a growing lobe. The key difference between the perithallus of

268   the *L. laeve* and *K. epilaeve* was the presence of wide (1-2 microns) areas of interfilament

269   in the *K. epilaeve* (Fig. 3A, F, 4A, B). In many corallines (Adey et al. 2005), including

270   the *L. laeve* studied for this paper there is only a single layer of interfilament grains, and

271   these present as vertical stripes on vertical fractures (Fig. 2B). EDS measurements were

272   taken for both the *K. epilaeve* cell wall and interfilament (Fig. 3A, B). As the interaction

273   volume of the EDS beam is ~ 3 microns (Methods) and the cell wall and interfilament

274   thickness range from 1-3 microns, the values measured for both may include small

275   amounts of the other, although every effort was made to place the beam on the widest

276   part of the appropriate band. A second set of measurements was taken for the *L. leave*

277   cell wall and interfilament using lower kV and the results are reported separately.

278

279   *Mg content*

280   Bulk whole sample content of Mg, determined by powder XRD was 10.8 mol% $MgCO_3$

281   (Mg/Ca 0.13). This XRD Mg content is within the range for average winter and summer

282   Mg contents for *Clathromorphum compactum* collected from Arctic Bay, Kingitok and

283   Quirpon (Halfar et al. 2011, 2013). The EDS-determined average Mg content ranged

284   from 9.1 (*K. epilaeve* Perithallial interfilament) to 16.7 mol% $MgCO_3$ (*L. leave* upper

285   Hypothallial cell wall), (Table 1, Fig.6). The highest measured individual Mg content,

286   19.6 mol% $MgCO_3$, was in the *L. leave* upper crust HCW. Generally the Mg content of

287   interfilament was lower than cell walls, and perithallial cell walls had the highest Mg

288   content. The lowest values were for the *K. epilaeve* PIF and PCW, 9.1 and 10.1 mol%

289    $MgCO_3$ respectively, not significantly different at significance level of 0.05 but are

290   significantly different at significance level of 0.1 (p= 0.068) (Table 2). Keeping in mind

291   the values for the cell wall and interfilament include a small amount of carbonate from

292   the other, we consider the p=0.068 result likely does represent a true significant

293   difference between the two. The PCW for the *L. laeve* was slightly higher at 11.2 and

294   12.9 mol% $MgCO_3$ (under and upper crust respectively), these were not significantly

295   different from each other (p=0.112). The combined average of the upper and under *L.*

296   *leave* cell walls (12.2 mol% $MgCO_3$) was significantly higher (p=0.025) than the *K.*

297   *epilaeve* cell wall. However, comparing only the *L. leave* cell wall of the under crust, the

298   same side as the *K. epilaeve,* there was no significant difference (p=0.124). The greatest

299   difference between the upper and under *L. laeve* crust was found between the hypothallial

300   cell walls. The under HCW averaged 12.3 mol% $MgCO_3$, whereas the upper HCW was

301   4.4 mol% higher at 16.7 mol% $MgCO_3$. The upper HCW was significantly higher than

302   the *L. leave* PCW's but not different from the transitional CW's (15.6 mol% $MgCO_3$).

303   Based on the graph in figure 5 this upper range of Mg would equate to temperatures

304   above 9.3°C, more than double the known summertime highs at the sampling site.

305

306   The results for comparison of the cell wall and interfilament grains in the *L. leave* using 7

307   kV showed the interfilament, 8.5 mol% $MgCO_3$ (n=6), was significantly lower (p=0.001)

308   than the cell wall, 11.1 mol% $MgCO_3$ (n=8).

309

310   **Structural features**

311   *Cell wall*

312   Within the radial Mg-calcite structure (PCW) of the *K. epilaeve*, a concentric banding

313   pattern is present (Fig. 7 A-C). The radial Mg-calcite grains are not always one

314   continuous long grain. The banding is aligned to the presence of organic fibrils that

315   appear regularly throughout the PCW (Fig. 7B). Organic fibrils, ~10 nm thick, are

316   parallel to the cell wall edges. These are spaced 30-40 nm apart throughout the middle of

317   the cell wall. It appears that the fibrils are mineralized. At the outer edges of the cell wall

318   the number of fibrils increases and appear as a dense mesh approaching a membrane (Fig.

319   7B, C) that is infilled with carbonate. The parallel fibrils are connected to the radial Mg-

320   calcite grains, appearing as if to continue through the grain (Fig. 7C), similar to fence

321   wire threading through fence posts at pre-defined spacing. There are also fibrils that

322   drape over the grains. Where the fibrils concentrate to a mesh, this is also calcified but

323   with smaller grains without regular shape. In the *K. epilaeve* interfilament (PIF), the

324   grains are aligned to the cell wall surface (Fig. 7C). Fibrils also run through the PIF and

325   attach to the interfilament grains but not with the regular pattern seen in the cell wall.

326   Looking at a cross section of the cell wall from the top down (Fig. 7D), the fibrils can be

327   seen to form a dense mesh.

328

329   Similar features are visible in the *L. laeve* PCW (Fig. 8A, B), although the organic fibrils

330   are not as well exposed. Possibly these cell wall grains are less susceptible to dissolution

331   in the etching treatment making it more difficult to expose the organic features. The

332   radial cell wall grains appear anchored to the external edge of the cell wall, immediately

333   adjacent the interfilament.

334

335   After etching for 20 minutes, more of the organic fibrils are exposed in the *K. epilaeve*

336   interfilament (Fig. 9A) revealing a porous membrane. PIF grains have angular edges in

337   contrast to the rounded sides of the cell wall grains. The *L. laeve* perithallial

338   interfilament has rice-grain shaped Mg-calcite flattened against the external side of the

339   cell wall (Fig. 9B) with attachment fibrils. Fibrils are visible stretching between the

340   flattened interfilament grains on adjacent cells (Fig. 9C).

341

342   Hypothallial cell walls at 200-500 nm wide are much thinner than perithallial cell walls

343   (Fig. 10 A-C). The HCW internal structure appears roughly radial (Fig. 10 A- C). But, the

344   radial structure is not always well developed with parts of the HCW exhibiting a distinct

345   break down the middle of the radial structures (Fig. 10C). There are fibrils parallel to the

346   cell wall appearing to go through the wall grains similarly to the perithallial cell walls.

347   Interfilament grains are present, as in perithallial cells (Fig. 10B, C).   The HCW wall can

348   have two clearly defined morphologies (Fig. 10C). The wall adjacent to the interfilament

349   is narrowest at ~200 nm, has closely spaced organic fibrils and is poorly calcified

350   compared to the inner part of the wall (300-400 nm wide) and appears more like a

351   mineralized membrane. The wider inner part of the cell wall has radial grains but without

352   the well-defined shape of the PCW radial grains. Similar to the perithallial cell walls,

353   there are fibrils appearing to thread through the hypothallial cell wall grains.

354

355   The transitional cells between the hypothallus and perithallus have features from both

356   types present (Fig. 10D). The cell walls can be narrow, <200 nm, poorly mineralized

357   similarly to the outer part of the hypothallial cell wall. Parts of the cell wall resemble the

358   perithallial cell walls, with radial grains and wall width of nearly 1 micron, although

359   along the same wall this changes to ~200 nm wide and a poorly mineralized membrane.

360   The parallel fibrils are also present within the transitional cell walls. Interfilament grains

361   are present comparably to those between hypothallial and perithallial cells.

362

363   **Discussion**

364   *Site temperature, ecology and growth*

365   The site of collection for this specimen (Fig. 1A) is a pavement of coralline encrusted,

366   roughly flat to ovoid shells and pebbles often with dish shapes. Many, such as the

367   specimen employed in this study have a concave surface (due to the original mollusk

368   shape). The benthic surface that we show in figure 1B is likely quite stable with time in

369   the moderate reversing tidal current environment of the site. The conceptacles of *L. leave*,

370   requiring considerable solar energy for construction; all appear on the upper side of the

371   specimen and further assist our determination of orientation. Since the sea ice does not

372   clear the area until late June or early July, solar energy has already peaked, by the time

373   the benthos at 15-17 m receives significant light. Effectively, the growing season is July

374   through November, and with a mean growing season temperature of < 2º C. Based on the

375   lateral growth rates (5-7 μm/day) found by Adey (1970), a season of lateral growth would

376   provide less than one mm of extension. As we discuss below, the vertical growth in this

377   species is slower than the lateral growth. The layering seen in figure 1B likely represents

378   4-5 years of vertical growth. At 80-100 μm of perithallial addition/year, this relates well

379   to the 100-200 μm /year found with extensive data in the same region for

380   *Clathromorphum compactum* (Adey et al. 2015b).

381

382   Considering that *Leptophytum leave* crusts can be many cm broad and rarely exceed 500

383   μm in thickness, except by overgrowing of earlier crusts, it can be assumed that after

384   initial formation, upwards perithallial growth is either very slow, perhaps limited by the

385   development of conceptacles for which considerable photosynthate must be dedicated. *L.*

386   *leave* is a deep water species (Adey 1966a, b, 1968, 1971) and requires little solar energy

387   to grow and carry out its life cycle; however, as shown by Adey (1970), the rate of

388   hypothallial extension falls with light reduction, and it would be expected that growth on

389   the underside of a shell-encased fragment would be present but less than that on the upper

390   surface.

391

392   *Temperature and magnesium*

393   One of the challenges using samples collected at a single point in time is that the growth

394   history cannot always be precisely tied to previous points in time and temperature. As

395   discussed in the previous section, this crust likely represents 4-5 years of growth. Thus

396   the XRD mol% $MgCO_3$ is an average for that period. The individual EDS measurement

397   spots cannot be tied to a particular time of year or temperature. However, the annual

398   temperature range is not large, estimated to be ~ 4 ºC across the growing season.

399

400   The EDS-determined average Mg content for each carbonate type had a range of 7.6

401   mol% MgCO$_3$, from 9.1 (*K. epilaeve* interfilament) to 16.7 mol% MgCO$_3$ (*L. laeve* upper

402   crust hypothallus). The *L. laeve* upper hypothallus has 84% more Mg than the *K. epilaeve*

403   interfilament. Although the exact time and temperature of formation for each component

404   is not known, the temperature range (~4 ºC) alone is highly unlikely to explain the Mg

405   difference. Studies on Mg content in CCA for temperature proxies have used regressions

406   with temperature records to determine a range of responses from 0.266 mol %

407   (Williamson et al. 2014), ~1.0 (Halfar et al. 2000; Darrenougue et al. 2013) to 1.76 mol%

408   MgCO$_3$ (Kamenos et al. 2008) per degree celsius of temperature increase. Only the

409   Kamenos et al. (2008) calibration is close to explaining the range here. However, that

410   calibration was for branches of the rhodolith *Lithothamnion glaciale*. Using temperature

411   calibrations for crust CCA in experimental treatments, where temperature was the only

412   condition changed (Diaz-Pulido et al. 2014; Nash et al. 2016), a calibration of 0.33

413   mol%/°C is obtained. This rate is in agreement with results from Williamson et al.

414   (2014), Chave and Wheeler (1964) and Adey (1965). Using 0.33, a shift of 7.6 mol%

415   equates to 23°C of change, nearly four times greater than the maximum annual range at

416   this site. The magnesium offsets in different parts of the crust are clearly aligned to

417   anatomical features and not controlled by temperature. Within these offsets there may

418   still be a response to temperature over the seasons, but it was beyond the capacity of this

419   study to investigate seasonal changes. It is noteworthy that the upper crust hypothallus

Biogeosciences
Discussions

Open Access

EGU

420   average of 16.7 mol% $MgCO_3$ is equivalent to new surface crust of tropical *Porolithon*

421   *onkodes* grown at 30° C (Diaz Pulido et al. 2014)

422

423   *Structural features*

424   There are three main types of calcified structures within the vegetative tissues of

425   *Leptophytum leave* and *Kvaleya epilaeve*: (1) the radial Mg-calcite within the cell walls

426   of the perithallium, (2) the interfilament in both the perithallium and hypothallium and

427   (3) the thin hypothallial cell walls. Each has distinctively different features and

428   magnesium content. The more elongate (and thinner-walled) cells of the hypothallus have

429   been reported for other species of Melobesioideae (Adey 1964, 1965, 1966a). However,

430   this is the first study to show that the internal cell wall Mg-calcite structure and their

431   magnesium content differs from perithallial cell wall. Probably these thinner elongated

432   hypothallial cell walls are a result of relatively rapid growth during lateral extension.

433   There are numerous examples documenting higher Mg in parts of crusts that have grown

434   faster during the warmer seasons (e.g. *Clathromorphum compactum* and *C. nereostratum*

435   by Adey et al. 2013). In this case there is no elevated temperature. The mechanistic

436   process by which more Mg is incorporated into the HCW and how this relates to growth

437   rate is not known.

438

439   *Calcification and photosynthesis*

440   The parasitic epiphyte *K. epilaeve* is not known to photosynthesize. The similarity of cell

441   wall and interfilament features to those of the photosynthesizing host, *L. leave*, suggests

442   that the precipitation of the Mg-calcite is not directly driven by photosynthesis as has

Biogeosciences
Discussions

443   been suggested for coralline algae (Ries 2010) and demonstrated for calcifying green

444   algae *Halimeda*, (e.g. Adey 1998, Sinutok et al. 2012). Rather, considering also the

445   evidence for continued calcification during the Arctic winter (Halfar et al. 2011, Adey et

446   al. 2013), it seems likely the first control is the provision of the organic substrate that

447   subsequently either becomes calcified or induces calcification. This does not negate the

448   possibility of increased calcification as photosynthetic rates increase (e.g. Borowitzka

449   1981).

450   *Banding and magnesium uptake*

451   The concentric banding of organic fibrils within the perithallial cell wall is interesting

452   from a magnesium perspective. The dominant visual morphological pattern is the radial

453   Mg-calcite crystals. In contrast, other work indicates the dominant pattern of Mg

454   distribution within the cell may be unrelated to the radial features. Concentric zonations

455   of higher Mg content have been shown, using back scatter electron imaging, in cell walls

456   of tropical *Porolithon onkodes* (Nash et al. 2011). Ragazzola et al. (2016) using

457   NanoSIMs, also showed clear concentric banding of Mg within summer cell walls of

458   *Lithothamnion glaciale*. These published observations together with the results in this

459   study suggest there could be a strong organic control on Mg distribution within the cell,

460   with this being related to the concentric fibrils. Possibly the fibril organics enable higher

461   Mg incorporation than the organics involved in the radial structures. Ragazzola et al.

462   (2016) further documented a decreased prominence of Mg banding in winter cells of *L*.

463   *glaciale* and for those grown in CO_2 enriched conditions. Results from our study offer an

464   insight as to possible temperature or CO_2-driven ultrastructure changes that may result in

465   decreased Mg content. If the banded fibrils observed in this study are normally similarly

466   present in the *L. glaciale,* then an absence of the Mg bands for their winter and elevated

467   CO_2 treatment suggests that these fibrils could either be absent, or the organic structure or

468   composition has changed and no longer enables elevated Mg.

469

470   *Relevance to Climate Archiving*

471   This study has several implications for climate archiving using corallines. Most

472   importantly, anatomical controls can override temperature influences on Mg composition.

473   Thus, any study of CCA for temperature archiving must take into account changes in

474   anatomy throughout the measured areas. While hypothallial areas can usually be easily

475   excluded from most climate archiving (but see Bougeois et al. 2015), less obvious

476   anatomically different tissues such as the elevated Mg transitional cell walls may not be

477   noticeable at low magnification. This may lead to a false positive result identifying such a

478   region as reflecting a time of higher temperature. As well as these tissue-scale differences,

479   the cellular scale differences may also need to be considered. Any seasonal change in

480   relative proportion of CW to IF can shift the [Mg] in absence of any temperature-

481   influenced change. For example if CW = 10 mol% $MgCO_3$ and IF = 8 mol% $MgCO_3$,

482   and crust changes from 90:10 CW:IF to 50:50 this would equate to a change in of 9.8 to 9

483   mol% for measurements of bulk crust (i.e. spot sizes larger than the cell size, or smaller

484   spot sizes averaged without reference to their anatomical placement). This change

485   equates to a 2-3 degrees using a temperature calibration of 0.33 mol% $MgCO_3$ °C. Should

486   the difference in cell wall and interfilament mol% $MgCO_3$ be larger, then the total

487   average will change more substantially. Furthermore, the bulk magnesium results for

488   different CCA species with differing proportions of cell wall:interfilament from the same

489   temperature environments will have a range of non-temperature related Mg content that is

490   controlled by the cell wall:interfilament. This change in structure, if seasonally correlated,

491   will be indirectly related to temperature, but there may be other influences such as light.

492   Thus, the best CCA temperature climate archives, as compared to seasonal archives, are

493   likely to be those with the least seasonally varying ultrastructure changes.

494

495   Understanding the combined contribution of anatomical and temperature changes to

496   measured magnesium may help explain the variation of Mg-temperature calibrations in

497   the published literature. Typically it is the rhodoliths that show the highest response of

498   Mg to temperature, e.g. *Lithothamnion glaciale* at 1- 1.76 mol% $MgCO_3$ (Halfar et al.

499   2000; Kamenos et al. 2008) per degree celsius of temperature increase compared to

500   *Clathromorphum compactum* at 0.7 mol% $MgCO_3$ (Halfar et al. 2010). The *L. glaciale*

501   has distinct seasonal changes shifting to a clear band of elongated cells during summer, in

502   contrast, anatomical changes in *C. compactum* (Adey et al. 2013) are not so extreme.

503

504   *Suggestions for improving analytical methods*

505   Our work is ongoing in this area of research and as more species and ultrastructure are

506   studied we expect to be able to provide more detailed guidance on utilizing Mg from

507   CCA for climate proxies. However, in the interim, there are several steps that could be

508   incorporated into routine analyses to improve the accuracy of Mg climate proxies. Firstly,

509   it should become a routine part of analyses that the ultrastructure is assessed to determine

510   if the ratio of cell wall to interfilament carbonate changes regularly with seasons. Second,

511   when possible as well as the larger spot sizes used in sampling transects, e.g. 10-20

512   microns, make discrete spot analyses using the smallest reliable interaction volume

513   possible to determine indicative Mg offsets between the cell wall and interfilament so

514   that this can be adjusted for if necessary, in the final interpretation. Third, ensure that

515   hypothallial growth is not included in sampling transects. Usually the basal hypothallus is

516   easily avoided, but secondary hypothallus and transitional cells may be harder to avoid

517   without careful SEM analysis.

518

519   **Conclusion**

520   It appears that within these CCA, there is a strong control on the uptake of Mg in relation

521   to the different anatomical components. This is in contrast to the suggestion by Ries

522   (2010), based on Mg:Ca in seawater manipulation experiments, that corallines exert little

523   or no control over their Mg uptake other than to specify the polymorph. It would be

524   interesting to identify if each of interfilament, perithallial and hypothallial cell walls

525   reacted similarly to changes in temperature and seawater Mg:Ca, or if there were

526   differences in anatomical controls. Crucially, it is necessary to keep in mind the

527   biological controls on Mg uptake when using CCA Mg changes as a climate proxy.

528

529   **Acknowledgments**

533

534   **References**

535   Adey, W. 1964. The Genus *Phymatolithon* in the Gulf of Maine. *Hydrobiologia*

536   24:377-420.

537   Adey, W. 1965. The Genus *Clathromorphum* in the Gulf of Maine. *Hydrobiologia*

538   26:539-573.

539   Adey, W. 1966a. The Genera *Lithothamnium, Leptophytum* (nov. gen.) and

540   P*hymatolithon* in the Gulf of Maine. *Hydrobiologia* 28:321-368.

541   Adey, W. 1966b. The Genus *Pseudolithophyllum* in the Gulf of Maine.

542   *Hydrobiologia* 27:479-597.

543   Adey, W. 1966c. The Distribution of Saxicolous Crustose Corallines in the

544   Northwestern North Atlantic. *J. Phycol.* 2:49-54.

545   Adey, W. 1970. The Effects of Light and Temperature on Growth Rates in

546   Boreal-Subarctic Crustose Corallines. *J. Phycol.* 6:269-276.

547   Adey, W. 1973. Temperature Control of Reproduction and Productivity in a

548   Subarctic Coralline Alga. *Phycologia* 12:111-118.

549   Adey, W. 1978a. Coral Reef Morphogenesis: A Multidimensional Model.

550   *Science* 202:831-837.

551   Adey, W. 1978b. Algal Ridges of the Caribbean Sea and West Indies. *Phycologia*

552   17:361-367.

553   Adey, W. 1998. Coral Reefs: algal structured and mediated ecosystems in shallow,

554   turbulent alkaline seas. *J. Phycol.* 34:393-406.

555   Adey, W. & D. McKibbin. 1970. Studies of the Maerl Species of the Ria de Vigo.

556   *Bot. Mar.* 8:100-106.

Biogeosciences
Discussions

Open Access
EGU

557   Adey, W. & C. Sperapani. 1971. The Biology of *Kvaleya epilaeve*, A New

558   Parasitic Genus and Species of Corallinaceae. *Phycologia* 10:29-42.

559   Adey, W., T. Masaki & H. Akioka. 1974.   *Ezo epiyessoense*, A New Parasitic Genus and

560   species of Corallinaceae. *Phycologia* 13:329-344.

561   Adey, W. & J. M. Vassar. 1975. Colonization, Succession and Growth Rates of

562   Caribbean Crustose Corallines. *Phycologia* 14:55-69.

563   Adey, W., Y. Chamberlain, & L. Irvine. 2005.   A SEM-Based Analysis of the

564   Morphology, reproduction and ecology of *Lithothamnion tophiforme* Unger

565   (Corallinales, Rhodophyta), an Arctic coralline. *J. Phycol.* 41:1010-1024.

566   Adey, W., Lindstrom, S., Hommersand M. & Muller, K. 2008. The biogeographic origin

567   of Arctic endemic seaweeds: A thermogeographic view. *J. Phycol.* 44:1384-1394.

568   Adey, W., Halfar, J. & Williams, B. 2013. The coralline genus *Clathromorphum* Foslie

569   emend Adey; biological, physiological and ecological factors controlling

570   carbonate production in an Arctic/Subarctic climate archive. *Smithsonian*

571   *Contributions to the Marine Sciences* 40:1-83.

572   Adey, W., Hernandez-Kantun, J. J., Johnson, G. & Gabrielson, P. 2015a. DNA

573   sequencing, anatomy and calcification patterns support a monophyletic, Subarctic,

574   carbonate reef-forming *Clathromorphu*m (Hapalidiaceae, Corallinales,

575   Rhodophyta). *J. Phycol.* 51:189-203.

576   Adey, W., Halfar, J., Humphreys, A. Belanger, D., Gagnon, P. & Fox, M. 2015b.

577   Subarctic rhodolith beds promote longevity of crustose coralline algal buildups

578   and their climate archiving potential. *Palaios* 30:281-293.

579   Amado-Filho, G., Moura, R., Bastos, A., Salgado, L., Sumida, P., Guth, A., Francini-

580   Filho, R., Pereira-Filho, G., Abrantes, D., Brasileiro, P., Bahia, R., Leal, R.,

581   Kaufman, L., Kleypas, J., Farina, M. & Thompson, F. 2012. Rhodolith Beds are

582   major CaCO3 bio-factories in the Tropical South West Atlantic. *Plos One* 7

583   (4):e35171.

584   Bahia, R., Abrantes, D., Brasileiro, P., Pereira-Filho, G. & Amado-Filho, G. 2010.

585   Rhodolith bed structure along a depth gradient on the northern coast of Bahia

586   State, Brazil. *Brazilian J. Oceanography* 58:323–337.

587   Barnes, D. J., & Lough, J. M. 1993. On the nature and causes of density banding in

588   massive coral skeletons. *J. Exp. Mar. Biol. Ecol.* 167:91-108.

589   Bentov, S., & Erez, J. 2005. Novel observations on biomineralization processes in

590   foraminifera and implications for Mg/Ca ratio in the shells. *Geology* 33:841-844.

591   Borowitzka, M. A. 1981. Photosynthesis and Calcificaton in the Articulated Coralline

592   Red Algae *Amphiroa anceps* and *A. foliacea*. Mar. Biol. 62:17-23.

593   Bougeois, L., Williams, B., Halfar, J., Konar, B., Adey, W., Kronz, A. & Wortmann, U.G.

594   2015. Does the coralline alga *Leptophytum fœcundum* (Kjellman) capture

595   paleoenvironmental variability in the Arctic Ocean? *Arctic, Antarctic, and Alpine*

596   *Research* 47:375-387.

597   Chave, K. & B. Wheeler. 1965 Mineralogical changes during growth in the red alga

598   *Clathromorphum compactum. Science* 147:621.

599   Darrenougue, N., De Deckker, P., Payri, C., Eggins, S., & Fallon, S. 2013. Growth and

600   chronology of the rhodolith-forming, coralline red alga Sporolithon

601   durum. *Marine Ecology Progress Series* 474:105-119.

602   Esau, K. 1953. Plant Anatomy. John Wiley and Sons. New York. 735 pp.

603   Nash, M. C., Opdyke, B. N., Troitzsch, U., Russell, B. D., Adey, W. H., Kato, A., Diaz-

604   Pulido G., et al. 2013. Dolomite-rich coralline algae in reefs resist dissolution in

605   acidified conditions. *Nat. Clim. Change* 3:268-272.

606   Halfar, J., Zack, T., Kronz, A., & Zachos, J. C. 2000. Growth and high-resolution

607   paleoenvironmental signals of rhodoliths (coralline red algae)- A new biogenic

608   archive. *J. Geophysical Research* 105:22-107.

609   Gamboa, G., Halfar, J., Hetzinger, S., Adey, W., Zack, T., B. Kunz, B., & Jacob, D. 2010.

610   Mg/Ca ratios in coralline algae as proxies for NW Atlantic temperature variations.

611   *J. Geophysical Research-Oceans* 115:1-12.

612   Halfar, J., Hetzinger, S., Adey**,** W., Zack, T., Gamboa, G., Kunz, B., Williams, B., Jacob,

613   D. 2010. Coralline algal growth increment widths archive North Atlantic climate

614   variability. *Palaeogeography, Palaoeoclimatology, Palaeoecology* 302:71-80

615   Halfar, J., Adey, W., Kronz, A., Edinger, E., & W. Fitzhugh, W. 2013. Unprecedented

616   sea-ice decline archived by novel multi-century annual-resolution algal proxy.

617   *PNAS* 110: 197837-19741.

618   Harvey, A. S., Harvey, R. M., & Merton, E. 2016. The distribution, significance and

619   vulnerability of Australian rhodolith beds: a review. *Marine and Freshwater*

620   *Research* doi.org/10.1071/MF15434.

621   Hetzinger, S., Halfar, J., Kronz, A., Steneck, R.S., Adey, W., Lebednik, P. A. & Schone,

622   B. R. 2009. High-Resolution Mg/Ca Ratios in a coralline Red Alga As a Proxy

623   for Bering Sea Temperature Variations from 1902-1967. *Palaios* 24:406-412.

Biogeosciences
Discussions

624   Kamenos, N., Cusack, M., & Moore, P. G. 2008. Coralline Algae Are Global

625   Paleothermometers with Bi-Weekly Resolution. *Geochimica et Cosmochimica*

626   *Acta* 72:771–779.

627   Kamenos, N. A., & Law, A. 2010. Temperature controls on coralline algal skeletal

628   growth. *J. Phycol.* 46:331-335.

629   Krayesky-Self, S., Richards, J., Rahmatian M., & Fredericq, S. 2016. Aragonite infill in

630   overgrown conceptacles of coralline Lithothamnion spp (Hapalidaceae,

631   Hapalidiales, Rhodophyta): new insights in biomineralization and

632   phylominerology. *J. Phycol.* 52:161-173.

633   Martin, C. S., Giannoulaki, M., De Leo, F., Scardi, M., Salomidi, M., Knittweis, L., Pace,

634   M. L. et al. 2014. Coralligenous and maërl habitats: predictive modelling to

635   identify their spatial distributions across the Mediterranean Sea. *Sci. Rep.* 4.

636   McCoy, S. J., & Kamenos, N. A. 2015. Coralline algae (Rhodophyta) in a changing

637   world: integrating ecological, physiological, and geochemical responses to global

638   change. *J. Phycol.* 51:6-24.

639   Nash, M. C., Troitzsch, U., Opdyke, B., Trafford, J., Russell, B., & Kline, D. 2011. First

640   discovery of dolomite and magnesite in living coralline algae and its

641   geobiological implications. *Biogeosciences.* 8, 3331-3340.

642   Nash, M. C., Opdyke, B. N., Wu, Z., Xu, H. & Trafford J. M. 2013. Simple X-ray

643   diffraction techniques to identify Mg calcite, dolomite, and magnesite in tropical

644   coralline algae and assess peak asymmetry. *J. Sed. Res.* 83:1085-1099.

645   Nash, M. C., Uthicke, S., Negri, A.P., & Cantin, N. E. 2015. Ocean acidification does not

646   affect magnesium composition or dolomite formation in living crustose coralline

647   algae, *Porolithon onkodes* in an experimental system. *Biogeosciences* 12:5247-

648   5260.

649   Nash M.C., Martin S., Gattuso J-P. 2016. Mineralogical response of the Mediterranean

650   crustose coralline alga *Lithophyllum cabiochae* to near-future ocean acidification

651   and warming. *Biogeosciences Discussions* doi:10.5194/bg-2016-160..

652   Ries, J. 2010. Review: Geological and Experimental Evidence for Secular Variation in

653   Seawater Mg/Ca (Calcite-Aragonite Seas) and Its Effects on Marine Biological

654   Calcification. *Biogeosciences* 7:2795–2849.

655   Sinutok, S., Hill, R., Doblin, M. A., Kühl, M., & Ralph, P. J. 2012. Microenvironmental

656   changes support evidence of photosynthesis and calcification inhibition in

657   *Halimeda* under ocean acidification and warming. *Coral Reefs* 31:1201-1213.

658   Sherman, C.E., Fletcher, C., Rubin, K., Simmons, K. & Adey, W. 2014. Sea-level and

659   reef accretion history of Marine Oxygen Isotope Stage 7 and late stage 5 based on

660   age and facies of submerged late Pleistocene reefs, Oahu, Hawaii. *Quaternary Res*.

661   81:138-150.

662   Wanamaker, A., Kreutz, K., Schone, B., Pettigrew, N., Borns, H., Introne, D., Belknap,

663   D., Maasch, K. & Feindel, S. 2008. Coupled North Atlantic slope water forcing

664   on Gulf of Maine temperatures over the past millennium. *Climate Dynamics*

665   31:183-194.

666   Williamson, C. J., Najorka, J., Perkins, R., M. L. Yallop, M. L. & Brodie, J. 2014.

667   Skeletal mineralogy of geniculate corallines: providing context for climate change

668   and ocean acidification research. *Marine ecology progress series* 513:71-84.

669

Biogeosciences
Discussions
Open Access
EGU

670   **Tables**

	K.epilaeve		*L. laeve*					
	IF	CW	CW Under	CW Upper	CW comb.	Under Hyp.	Upper transit.	Upper Hyp.
mol% MgCO₃	9.1%	10.1%	11.2%	12.9%	12.2%	12.3%	15.6%	16.7%
St. Dev.	1.0%	1.2%	1.2%	2.5%	2.2%	0.7%	1.7%	1.7%
Mg/Ca	0.100	0.113	0.126	0.149	0.138	0.140	0.185	0.200

671   **Table 1: SEM-EDS results. Conversion of mol% to Mg/Ca is included.**

	Average mol% and n	*K. epilaeve* IF	*K. epilaeve* CW	*L. laeve* under CW	*L. laeve* upper CW	*L. leave* CW both	*L. laeve* under Hyp.	*L. laeve* upper Hyp.
K. epilaeve IF	9.1 % n=9							
K. epilaeve CW	10.1% n=8	**0.069**						
L. laeve under CW	11.2% n=8		0.129					
L. laeve upper CW	12.9% n=9		**0.012**	0.112				
L. leave CW both	12.2% n=17		**0.024**					
L. laeve under Hyp.	12.3% n=8			**0.052**	0.470	0.914		
L. laeve upper Hyp.	16.7% n=8					**<0.001**	**<0.001**	
L. laeve upper trans.	15.6% n=8					**<0.001**	**<0.001**	0.259

672   **Table 2: T-test *p* values for 15 kV spot EDS.**

673

674   **Figures**
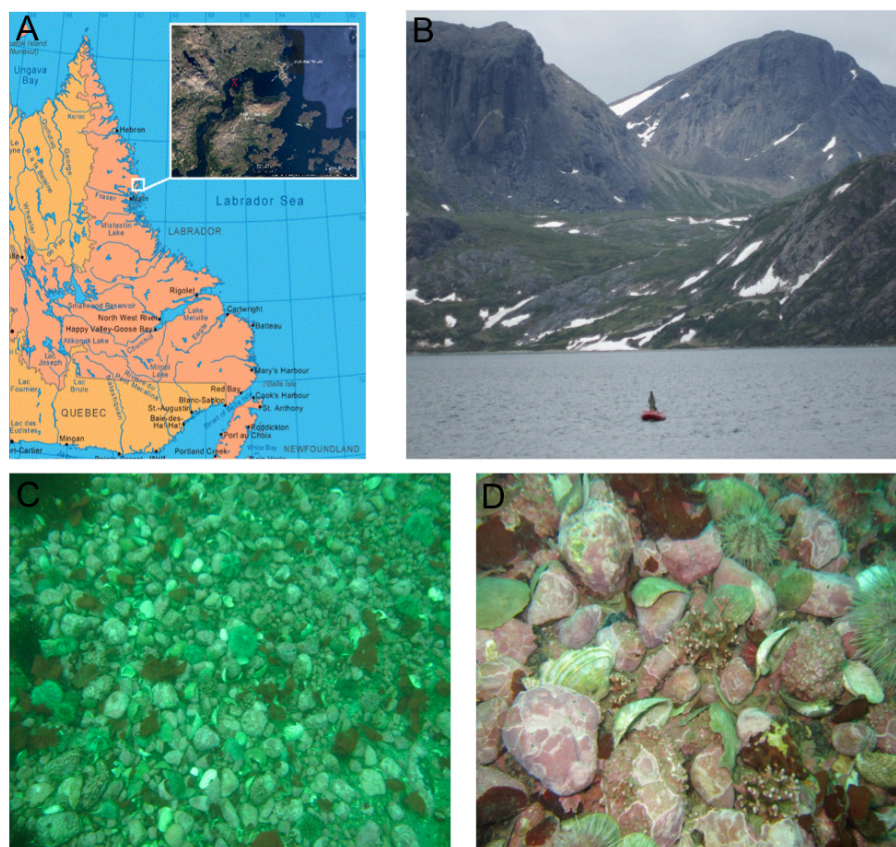
675

676   Figure 1: A. Port Manvers Bay Station, Labrador. B. Collecting site in western Port Manvers Bay. C.

677   Pebble/shell bottom with occasional rhodoliths at 15-17 m. Coralline covered pebbles range from about 5-

678   10 cm diameter. D. Close-up of bottom shown in figure 1C.

679
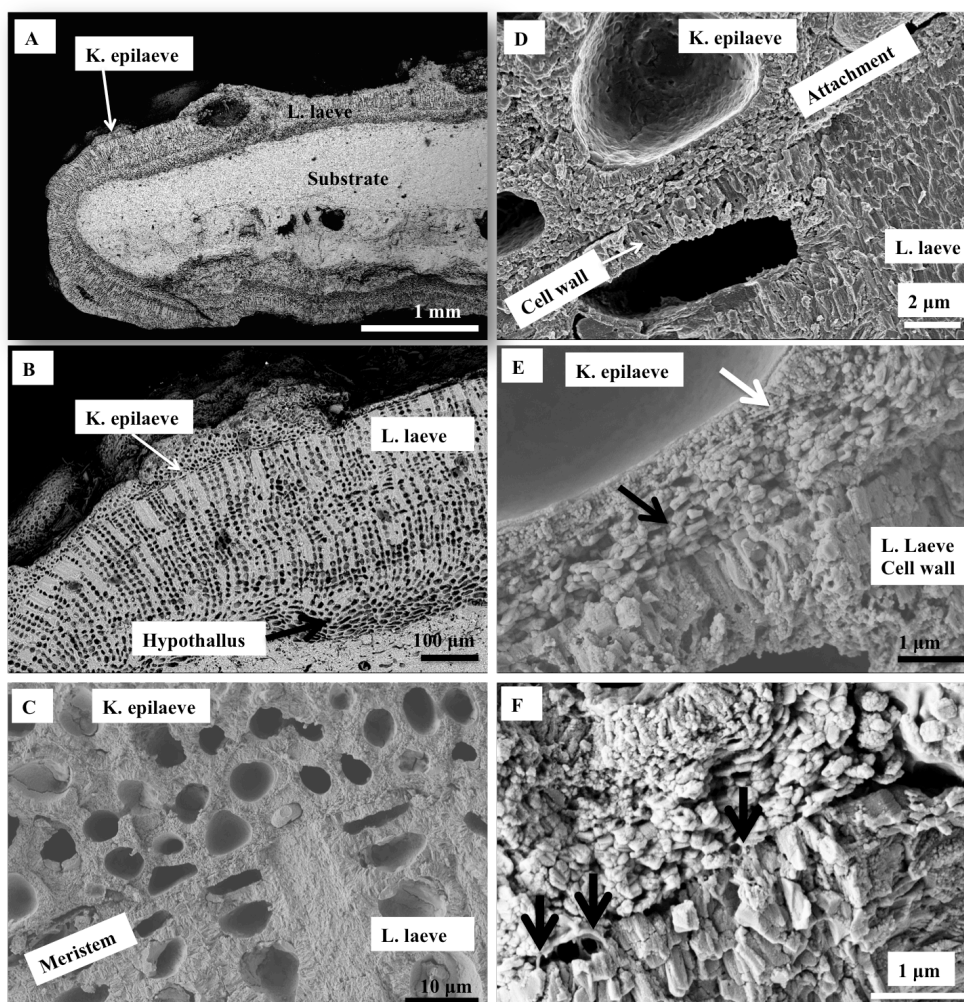
Figure 2: Overview of *K. epilaeve* on *L. laeve*. **A**. Overview (BSE). *L. laeve* has been partly overgrown by

K. epilaeve. **B**. Closer up (BSE) *K. epilaeve* has a very thin perithallium with thicker buildup for its

conceptacle. **C**. Close up (SE) and **D** showing attachment zone of *K. epilaeve* hypothallus on the meristem

of the *L. laeve*. **E**. (SE) The cell wall in the *L. laeve* is roughly radial whereas the *K. epilaeve* cell wall does

not appear properly mineralized with nm-scale beads of Mg-calcite along what appears to be organic fibrils

(white arrow). The *K. epilaeve* Mg-calcite layer at the attachment zone has coarse angular grains roughly

parallel to the *L. laeve* surface (black arrow). **F**. (SE) Organic fibrils are visible (black arrows) between the

base of the *K. epilaeve* and the surface of the *L. laeve* suggesting this is the attachment mechanism.

688
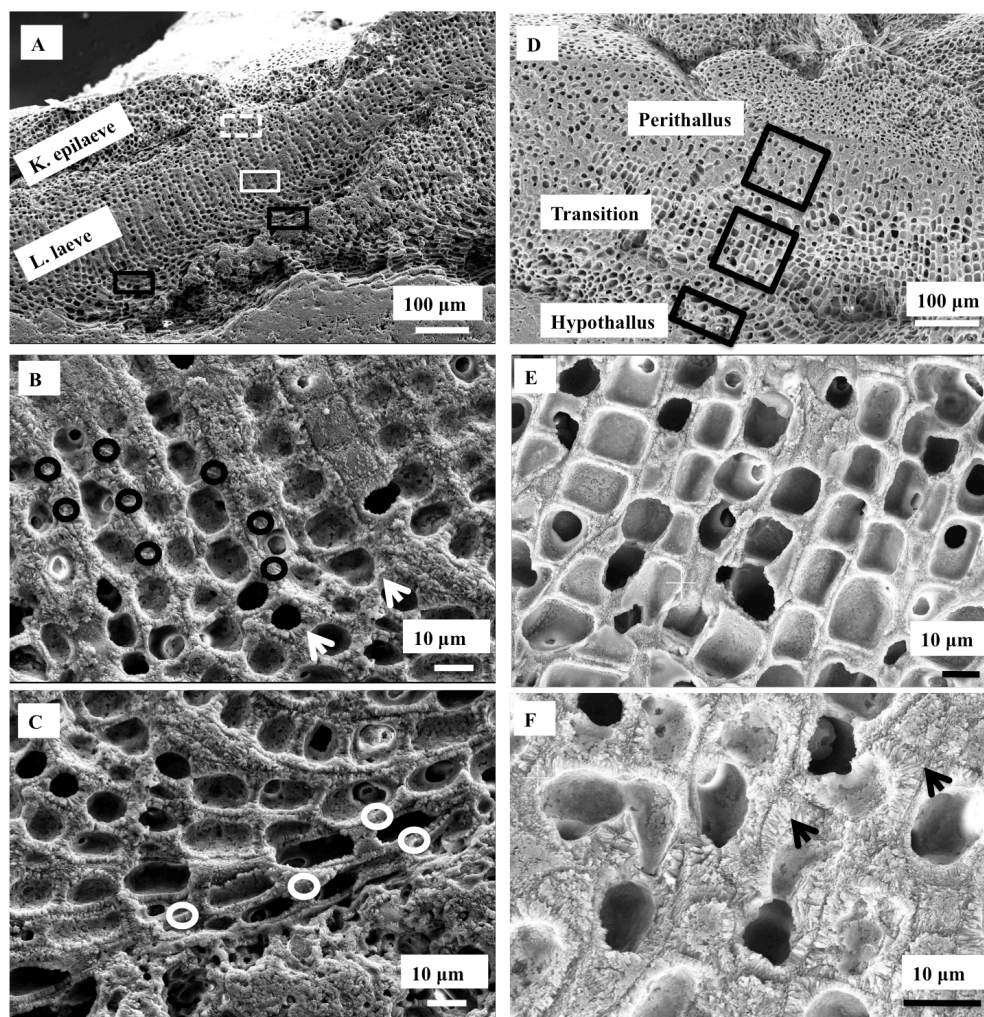
Figure 3: Overview of *L. laeve* and *K. epilaeve* and EDS sites in *L. laeve*. **A-C**. Sites on the underside of the pebble. **D-F**. Sites on the upper side of the pebble. **A**. White dashed box- cell wall and interfilament in *K. epilaeve*. White box– perithallial cell wall *L. laeve*. Black box- hypothallus *L. laeve*. **B**. EDS sites for cell wall measurements of *L. laeve*. Circle size indicates approximate area of measurement (3 microns). Cell wall radial Mg-calcite (arrowheads). **C**. EDS sites for hypothallus (right box in A). **D**. EDS sites on sample upper side for *L. laeve*. E. *L. leave*. **F**. *L. leave*. Cell walls in upper side are visually comparable to cell walls in underside with radial Mg-calcite (arrowheads) in cell walls and minimal interfilament.
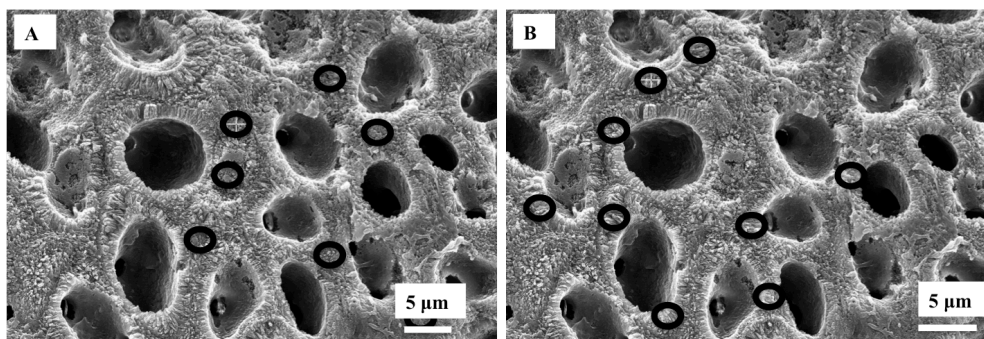
696

697   Figure 4: Detail of EDS in *K. epilaeve* (dashed white box in Fig. 2A) **A**. EDS sites for interfilament. **B**.

698   EDS sites for cell wall.

699
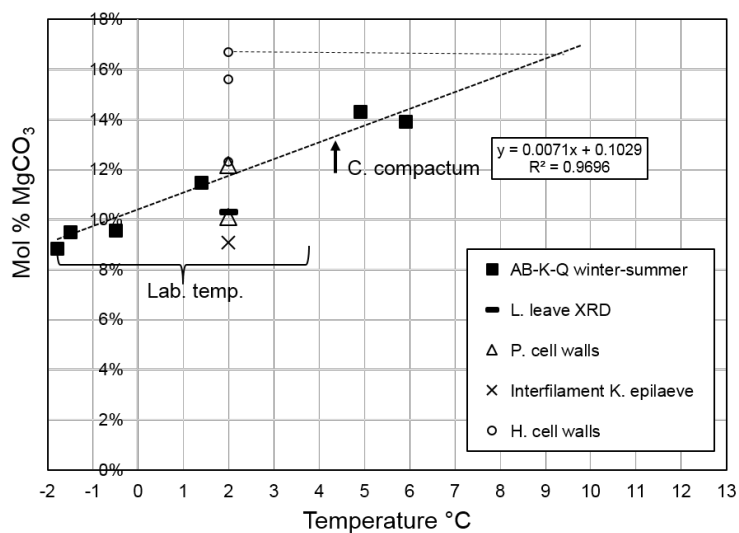
700

701   Figure 5: *L. Leave* and *K. epileave* Mg content relative to *Clathromophum compactum* from Arctic Bay,

702   Kingitok and Quirpon (Halfar et al. 2010, 2013). Lab – Labrador sea. Heavy dashed line- best fit for *C.*

703   *compactum*. Light dashed line- indicates the temperature equivalent on the *C. compactum* line for the L.

704   leave hypothallial Mg-content.

705

Biogeosciences
Discussions

Open Access

EGU

706
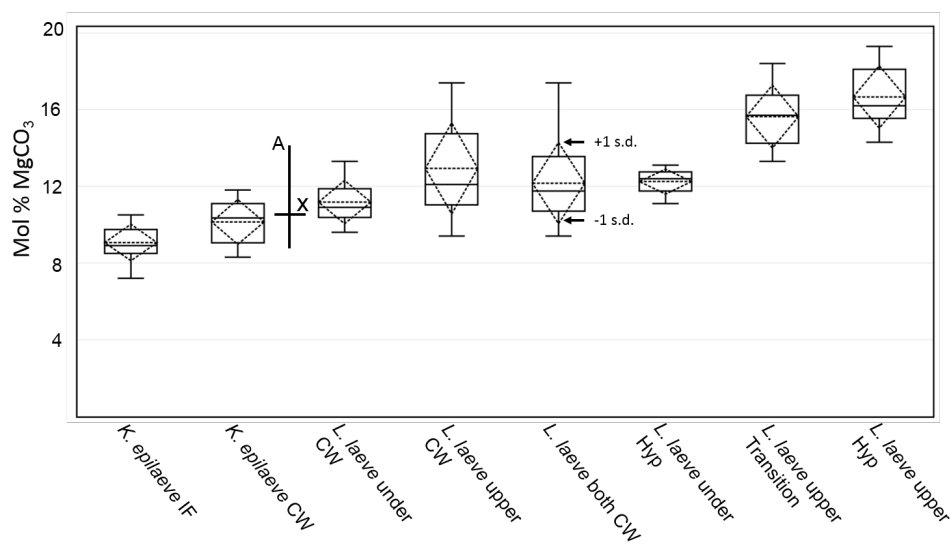
Figure 6: Box plot of EDS mol% MgCO$_3$ results. Box represents the 2nd and 3rd quartiles. The lower and

upper bars are the minimum and maximum values (excluding an outlier for *L. laeve* under cell wall). The

solid middle line within the box is the median value and the dash middle line the average. The dashed

diamond box represents one standard deviation. The drawn-on cross represents the XRD mol% (X) and the

seasonal range (A) of mol% for the Arctic Bay – Kingitok – Quirpon dataset in figure 5.

712

Biogeosciences
Discussions

Open Access

EGU

713
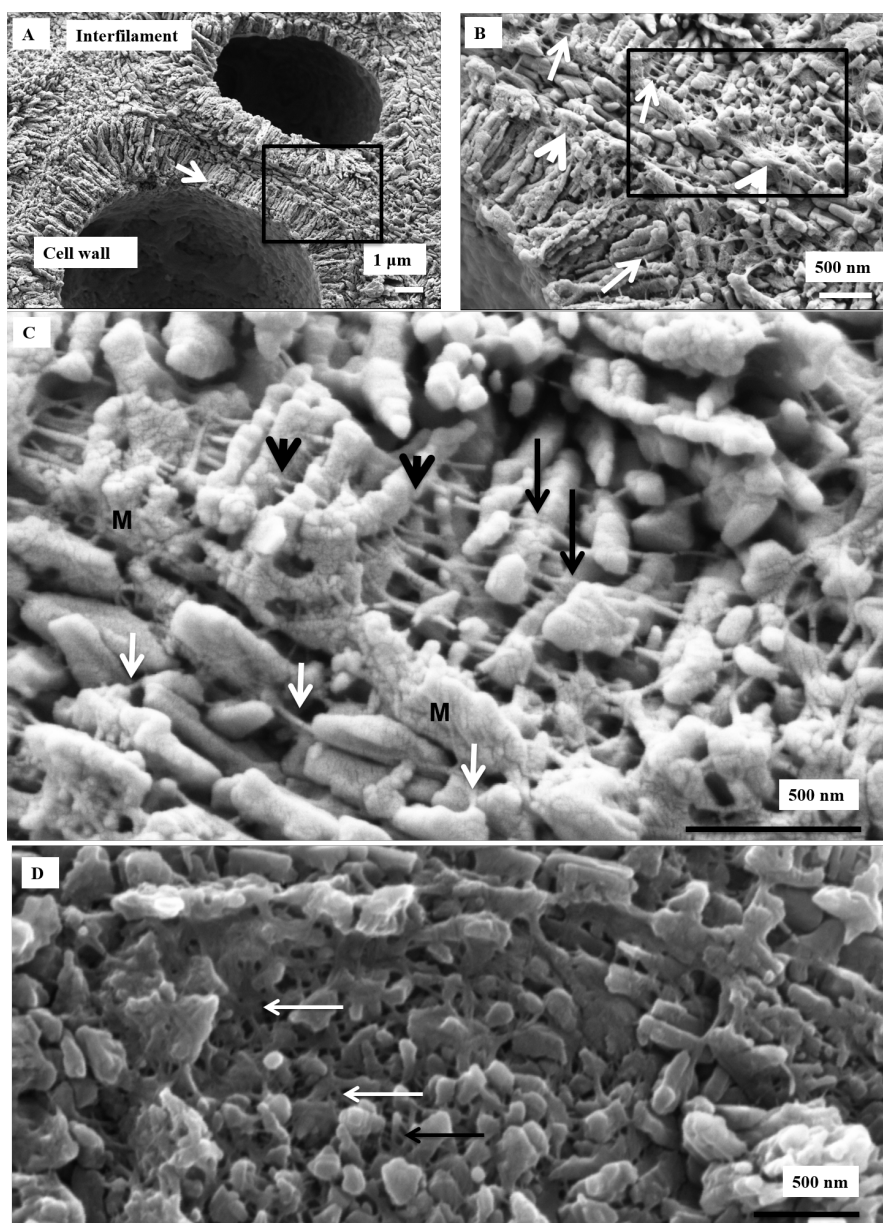
Figure 7: *K. epilaeve* cell wall structure. Crust polished and cleaned for 2 minutes. **A**. Cell walls have radial

Mg-calcite whereas the interfilament grains are orientated either parallel to the filament axis or randomly

within the corner junctions. Within the radial cell walls a secondary concentric banding pattern is visible

(white arrow). Black box enlarged in B. **B**. Organic fibrils, ~10nm wide, run parallel to cell wall edges

718 (black arrows). Fibrils are concentrated along the outer of the cell wall (white arrows). Black box enlarged

719 in C. **C**. The cell wall fibrils appear to string through the centre of the radial grains (black arrowheads),

720 Other fibrils drape over the grains (black arrows). Fibrils are present in the interfilament (white arrows). M

721 – mineralized membrane. **D**. Plan view of cell wall grains. Organic fibrils form a dense mesh (white

722 arrows).

723
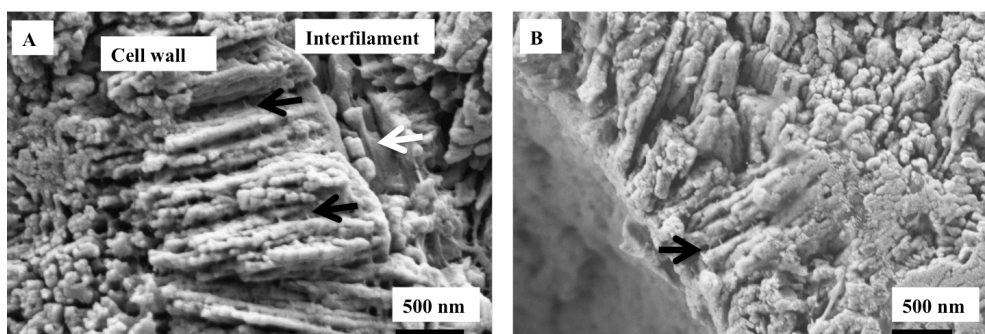
724

725 Figure 8: *L. laeve* cell wall structure. A. Cleaned for 2 minutes. Cell wall radial crystals are 1.5 micron

726 length cylindrical grains. Fibrils are present (black arrows) but not as easy to see as in the *K. epilaeve*.

727 Interfilament grains parallel to cell wall with organic fibrils (white arrows) also running parallel to cell wall.

728 B. Etched for 20 minutes. Fibrils appear similarly as in the *K. epilaeve* with the fence post-wire structure

729 (black arrows).

730

731
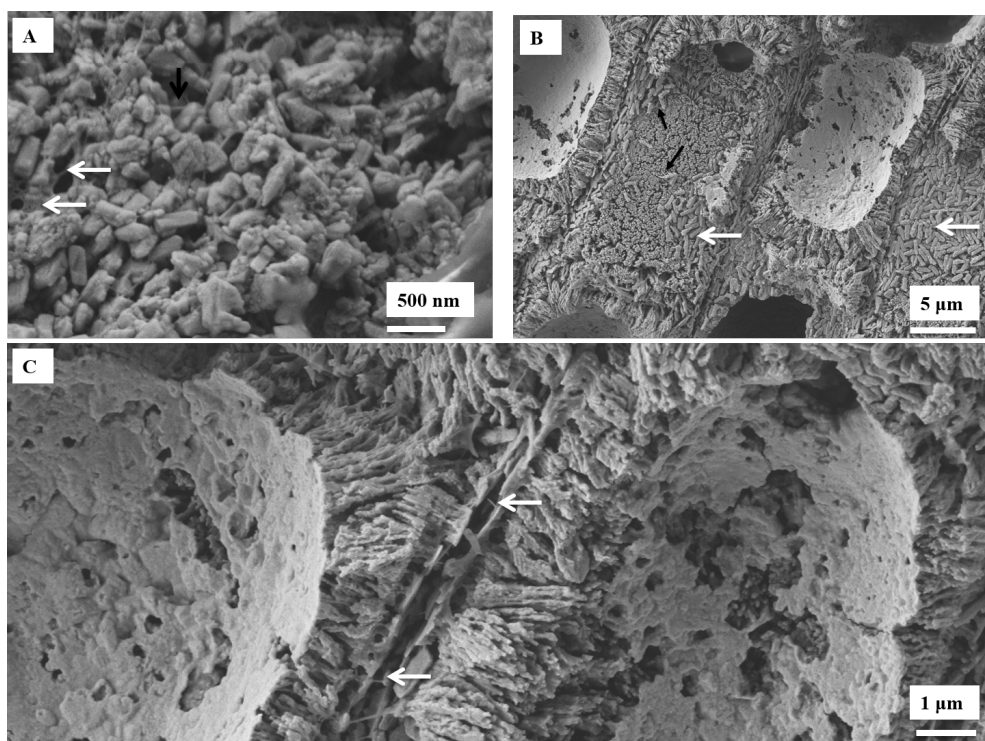
Figure 9: Interfilament structures in *K. epilaeve* (A) and *L. laeve* (B, C). **A**. *K. epilaeve* etched for 20

minutes. Fibrils (black arrow) and porous membrane (white arrows). **B**. *L. Laeve* etched for 20 minutes.

Interfilament grains are flattened against the external sides of the cell wall (white arrows) attached by

fibrils (black arrows). **C**. Fibrils visible stretched across the space between cell walls with 2 layers of

interfilament grains (white arrows).

737

738
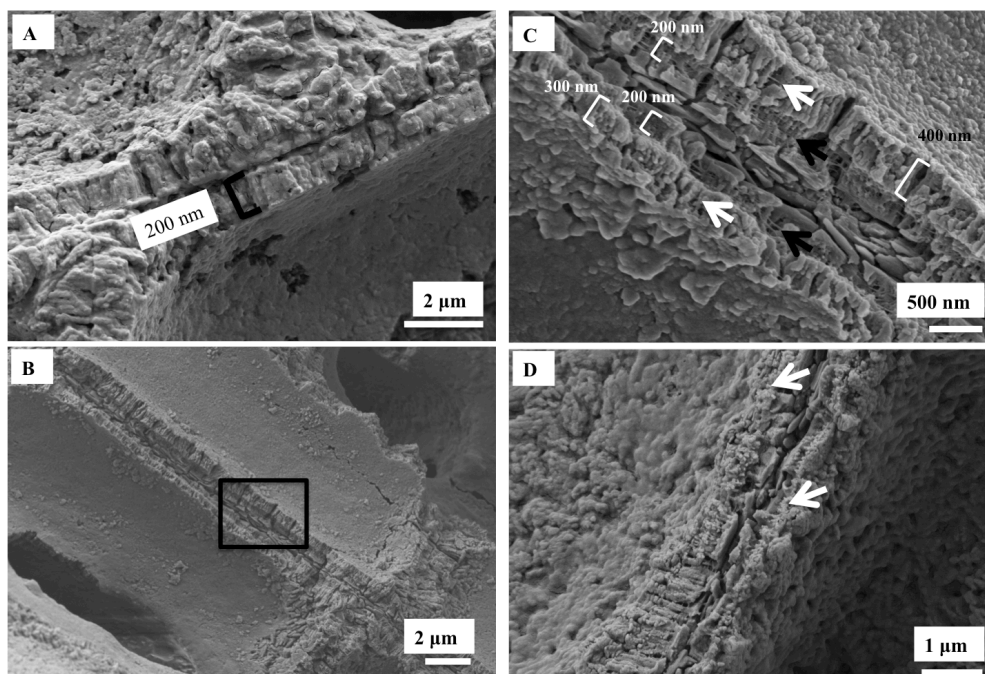
Figure 10: Hypothallus and transitional cells in *L. leave*. Cleaned 2 minutes. **A**. Hypothallus underside.

Organic film covering wall structures. Walls ~200 nm wide, roughly radial structure within cell wall. **B**.

Cleaned 2 minutes, hypothallus in upper crust. Roughly radial structure within cell walls. Black box

enlarged in C. **C**. The wall adjacent to the interfilament is narrowest at ~200 nm, has closely spaced organic

fibrils (black arrows) and is poorly calcified compared to the inner part of the wall (300-400 nm wide)

where radial grains are present. There are fibrils parallel to the cell wall appearing to go through the wall

grains similarly to the perithallial cell walls (white arrows). **D.** Transitional cell wall. The calcification in

the lower of the left side wall is comparable to the perithallial cell wall with radial grains. The right side

wall and upper part of the left side (white arrows) are poorly calcified and appear as a calcified membrane

rather than a properly developed cell wall.

749